Research Articles

GREENSUSMATER

Greensusmater
Vol. 3, No. 1, 2026
https://doi.org/10.62755/gsm.2026.05

Check for updates

Effect of Composition and Morphology of Electrospun Polyacrylonitrile/Polyvinylpyrrolidone (PAN/PVP) Nanofibers on Adsorption of Methylene Blue and Congo Red Dyes

Istiara Rizqillah Hanifah[1,*], Alex Triputra Lumban Tobing[1], Hanna Ronauli Permata Simamora[1], Anisa Fitri[1], Agita Phasa[1]

[1] *Department of Materials Engineering, Faculty of Industrial Technology, Institut Teknologi Sumatera, Terusan Ryacudu, Way Hui, Jati Agung, Lampung Selatan 35365, Indonesia*

Corresponding author: istiara.hanifah@mt.itera.ac.id

ARTICLE HISTORY: Received: April 18, 2026 | Revised: May 9, 2026 | Accepted: May 13, 2026

ABSTRACT

Synthetic dyes such as methylene blue (MB) and Congo red (CR) are persistent water pollutants requiring efficient removal. This study examines the effect of composition and morphology on the adsorption performance of electrospun polyacrylonitrile/polyvinylpyrrolidone (PAN/PVP) nanofiber membranes. PAN/PVP fibers with different PAN loadings (0.7–1.0 g, total polymer mass 1.3 g) were fabricated by electrospinning and subjected to hot-water soaking at 80 °C followed by thermal treatment at 200 °C. SEM and FTIR confirmed continuous nanofibrous networks containing both PAN and partially removed PVP, with only subtle morphological differences among compositions. Batch adsorption tests showed preferential uptake of MB over CR, with the highest MB capacity of 8.38 mg g^{-1} obtained for the PAN/PVP-8 membrane and the highest CR capacity of 3.32 mg g^{-1} obtained for the PAN/PVP-10 membrane, with only modest variation among the other ratios. Kinetic analysis revealed that MB and CR adsorption follow a pseudo-second-order model, indicating surface-controlled uptake and suggesting that further improvement will require targeted surface functionalization.

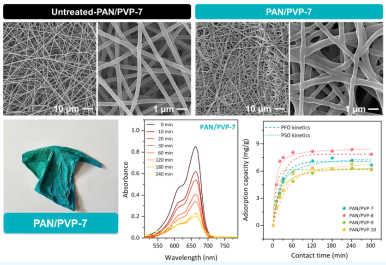

Keywords: *PAN/PVP nanofibers; Electrospinning; Morphology; Dye adsorption; Methylene blue; Congo red; Wastewater treatment*

1. INTRODUCTION

The discharge of textile wastewater has emerged as a major contributor to global water pollution [1]. The textile industry accounts for approximately 54% of hazardous organic pollutants, and it is estimated that 15–20% of synthetic dyes used in textile processing are not adequately treated and are subsequently released into the environment [2,3]. Globally, this corresponds to nearly 280,000 tons of dyes entering water bodies annually, leading to severe water contamination and posing significant risks to human health and aquatic ecosystems [4]. These dyes are commonly classified into cationic and anionic types [5]. Among them, methylene blue (MB) is one of the most widely used cationic textile dyes and is frequently detected in effluents due to its high stability and persistence [6]. Congo red (CR), an anionic azo dye widely used in the textile industry, is likewise often found in wastewater and is known for its potential toxicity and long-term environmental persistence. Therefore, the removal of hazardous dyes such as MB and CR from textile wastewater is of critical importance [7].

Various techniques have been explored for the removal of MB and CR from wastewater, including coagulation/flocculation, ion exchange, photodegradation, membrane filtration, and adsorption [8,9]. Among these methods, adsorption stands out as an effective and extensively studied approach owing to its simplicity, relatively low cost, and high removal efficiency. However, the overall performance of the process is strongly governed by the physicochemical properties of the adsorbent material, such as its surface area, porosity, surface chemistry, and stability [10].

Advances in nanotechnology have led to increasing use of nanostructured adsorbents for the removal of organic pollutants from aqueous media. In particular, electrospun polymeric nanofibers have attracted considerable attention due to their high specific surface area, interconnected porosity, and tunable morphology, all of which are beneficial for adsorption-driven separation processes [11]. Polyacrylonitrile (PAN) is widely employed in water treatment applications because of its chemical and mechanical stability, nontoxicity, and ease of surface functionalization. Its porous structure can be tailored by incorporating pore-forming agents such as polyvinylpyrrolidone (PVP), which can increase pore density while maintaining pore size and distribution [12,13,14,15,16,17,18,19,20].

While PAN/PVP fibrous materials have been investigated for various separation and removal applications, the interplay between blend composition, post-treatment–induced changes in PVP content, nanofiber morphology, and dye adsorption behaviour, particularly for representative cationic and anionic dyes such as MB and CR, remains insufficiently understood. In this context, the present work focuses on

PAN/PVP electrospun nanofiber membranes with different PAN/PVP ratios subjected to hot-water soaking and subsequent thermal treatment. The influence of these parameters on nanofiber morphology and chemical structure is examined by SEM and FTIR, and their impact on the adsorption performance toward MB and CR is evaluated through equilibrium and kinetic studies. By correlating the partial removal of PVP, the broadly similar morphologies, and the adsorption behaviour described by pseudo-second-order kinetics, this study aims to clarify the extent to which variations in PAN/PVP ratio and post-treatment affect dye uptake, and to identify the most promising PAN/PVP formulation as a platform for further performance enhancement via surface modification.

2. MATERIALS AND METHODS

2.1 Materials

Polyacrylonitrile (PAN, M_w = 150,000 g/mol) and polyvinylpyrrolidone (PVP, M_w = 1,300,000 g/mol) were purchased from Sigma-Aldrich and used to prepare polymer blend solutions, with *N*,*N*-dimethylformamide (DMF, Merck, Germany) as the solvent. Methylene blue (MB) and Congo red (CR) were employed as model dyes for the adsorption studies and purchased from Merck, Germany. Deionized water was used for the preparation of dye solutions and for all rinsing procedures.

2.2 Preparation of PAN/PVP nanofibers

Electrospinning solutions were prepared by varying the mass ratio of PAN to PVP while keeping the total polymer mass constant at 1.3 g. The PAN:PVP ratios used were 54:46, 62:38, 69:31, and 77:23, corresponding to PAN masses of 0.7, 0.8, 0.9, and 1.0 g, respectively (see Table 1). Each solution was magnetically stirred at 500 rpm and 60 °C for 3 h, until a homogeneous polymer solution was obtained. The prepared polymer solution was loaded into a 10 mL Terumo syringe equipped with a 21G needle and mounted on a syringe pump connected to an electrospinning apparatus (ILMI-N101 Electrospinning). The electrospinning process was carried out at an applied voltage of 9 kV and a flow rate of 1 mL h^{-1}. The distance between the needle tip and the collector was fixed at 15 cm. The collector, covered with aluminium foil, was designed as a rotating drum to ensure uniform fibre deposition on the substrate. After the nanofibre mats were obtained, they were subjected to post-treatment. The samples were immersed in distilled water at 80 °C for 2 h and then dried at room temperature until completely dry. The dried nanofibres were subsequently thermally treated in a tube furnace at 200 °C for 2 h, with a heating rate of 3 °C min^{-1}, under a nitrogen (N_2) atmosphere.

Table 1. Composition of PAN/PVP electrospinning solutions with varying PAN:PVP mass ratios for nanofibre preparation.

Sample name	PAN mass (g)	PVP mass (g)	DMF volume (mL)	PAN:PVP ratio
PAN/PVP-7	0.7	0.6	10	54:46
PAN/PVP-8	0.8	0.5	10	62:38
PAN/PVP-9	0.9	0.4	10	69:31
PAN/PVP-10	1.0	0.3	10	77:23

2.3 Materials characterization

The morphology of the electrospun PAN/PVP membranes was examined using scanning electron microscopy (SEM, JEOL JSM-6510). The chemical composition and functional groups were analysed by Fourier-transform infrared (FTIR) spectroscopy using a Shimadzu IRSpirit-X compact spectrometer in the range of 4000–500 cm^{-1} under ATR mode.

2.4 Adsorption investigations

The dye removal performance of the nanofibre membranes was evaluated using MB and CR dyes, representing cationic and anionic dyes, respectively. For each experiment, 0.05 g of the nanofibre membrane was immersed in 100 mL of MB or CR solution at an initial concentration of 5 ppm in a 100 mL glass beaker. Before the membrane was added, a 5 mL aliquot of the dye solution was withdrawn to determine the initial concentration (C_0). The adsorption experiments were conducted under dark conditions (in the absence of light) with continuous stirring at 400 rpm. At predetermined time intervals of 10, 20, 30, 60, 120, 180, 240, and 300 min, samples were withdrawn to determine the residual dye concentration. Each collected sample was transferred into a vial using a micropipette and analysed by UV–Vis spectrophotometry at wavelengths of 663 nm for MB and 498 nm for CR. For the quantitative evaluation of dye uptake, the dye concentrations at each sampling time were determined from a standard calibration curve (2, 5, 6, 8, and 10 ppm) obtained by UV–Vis spectrophotometry. The absorbance values measured at the characteristic wavelength of each dye were converted to concentration using this calibration plot. Based on these concentration values, the adsorption capacity at time t (q_t, mg g^{-1}) was calculated using the standard mass balance equation (Eq. 1):

$$q_t = \frac{(C_0 - C_t)\,V}{m} \tag{1}$$

where C_0 and C_t (mg L^{-1}) are the initial and time-dependent dye concentrations, respectively, V (L) is the solution volume, and m (g) is the membrane mass. After equilibrium was reached, the residual dye concentration (C_e) was determined spectrophotometrically, and the equilibrium adsorption capacity (q_e, mg g^{-1}) was calculated accordingly.

The kinetic behaviour of MB adsorption on the PAN/PVP nanofibre membranes was evaluated using the pseudo-first-order (PFO) and pseudo-second-order (PSO) kinetic models, which are widely applied in dye adsorption studies. The linear form of the PFO model is expressed as (Eq. 2):

$$\ln(q_e - q_t) = \ln q_e - k_1\,t \tag{2}$$

where q_e and q_t (mg g^{-1}) are the adsorption capacities at equilibrium and at time t, respectively, and k_1 (min^{-1}) is the PFO rate constant. The corresponding linear form of the PSO model is (Eq. 3):

$$\frac{t}{q_t} = \frac{1}{k_2\,q_e^2} + \frac{t}{q_e} \tag{3}$$

where k_2 is the PSO rate constant (g mg^{-1} min^{-1}).

3. RESULTS AND DISCUSSION

The SEM images in Figure 1a,b confirm the successful formation of continuous PAN/PVP nanofibre membranes by electrospinning. At low magnification (Figure 1a), all

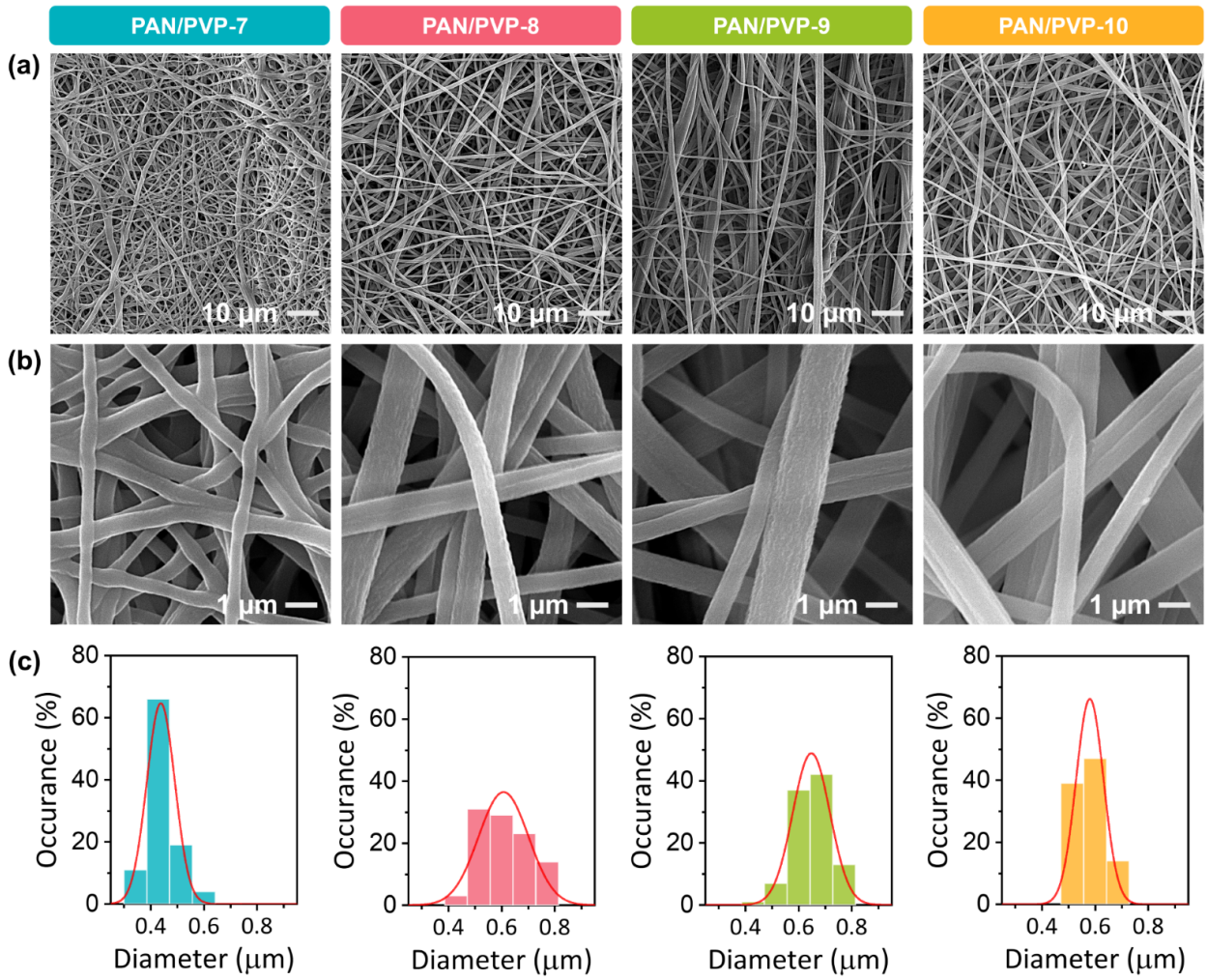

Figure 1. SEM images of electrospun PAN/PVP nanofibre membranes at different magnifications: (a) 1000×, (b) 10 000×, and (c) the corresponding fibre diameter distribution.

compositions (PAN/PVP-7, PAN/PVP-8, PAN/PVP-9, and PAN/PVP-10) display highly entangled, three-dimensional nanofibrous networks. The mats appear homogeneous over the observed areas without macroscopic defects or film-like regions. Higher-magnification images (Figure 1b) reveal that the individual fibres possess smooth surfaces and well-defined cylindrical shapes, with no noticeable bead formation or fused regions, indicating stable jet formation and adequate spinnability of the polymer solutions [13]. The corresponding diameter distributions are presented in Figure 1c. Fibre diameters were determined from 100 measurement points for each sample using ImageJ software applied to the SEM micrographs. Quantitative analysis shows that the average fibre diameters for PAN/PVP-7, PAN/PVP-8, PAN/PVP-9, and PAN/PVP-10 are 0.44 ± 0.05 µm, 0.61 ± 0.09 µm, 0.65 ± 0.07 µm, and 0.58 ± 0.05 µm, respectively. These values confirm that all samples remain within a comparable submicrometer diameter range, with only moderate variation in mean diameter among the different PAN/PVP ratios.

Direct SEM comparison between untreated and post-treated PAN/PVP-7 nanofibre membranes (Figure 2a) reveals that the overall fibrous network is largely preserved, but subtle morphological changes do occur. The untreated sample exhibits smooth, straight fibres with well-separated junctions [21], whereas the post-treated membrane shows slightly wrinkled fibre surfaces and occasional fused contact points at fibre intersections [22]. These features suggest a mild thermally induced relaxation of the PAN/PVP chains and local softening of the PVP-rich phase during the stabilization step, rather than severe melting or collapse of the network. Despite this partial wrinkling and junction fusion, the mats remain highly porous and continuous, with no evidence of extensive bead formation or large-scale densification. Consequently, post-treatment can be considered to introduce only minor morphological modifications, which are not sufficient to dominate the macroscopic methylene blue adsorption behaviour when compared with the concurrent changes in composition and surface chemistry.

Figure 2b compares the FTIR spectra of untreated and post-treated PAN/PVP-7 nanofibre membranes. The untreated sample exhibits a relatively intense and broad band in the 3600–3000 cm^{-1} region, attributed to O–H stretching vibrations from adsorbed moisture and water-soluble species associated with PVP [23]. After hot-water washing and thermal stabilization, the intensity of this O–H band decreases, indicating partial removal of physically adsorbed water and loosely bound hydrophilic residues. At the same time, the nitrile band of PAN at 2243 cm^{-1} (C≡N stretching) retains

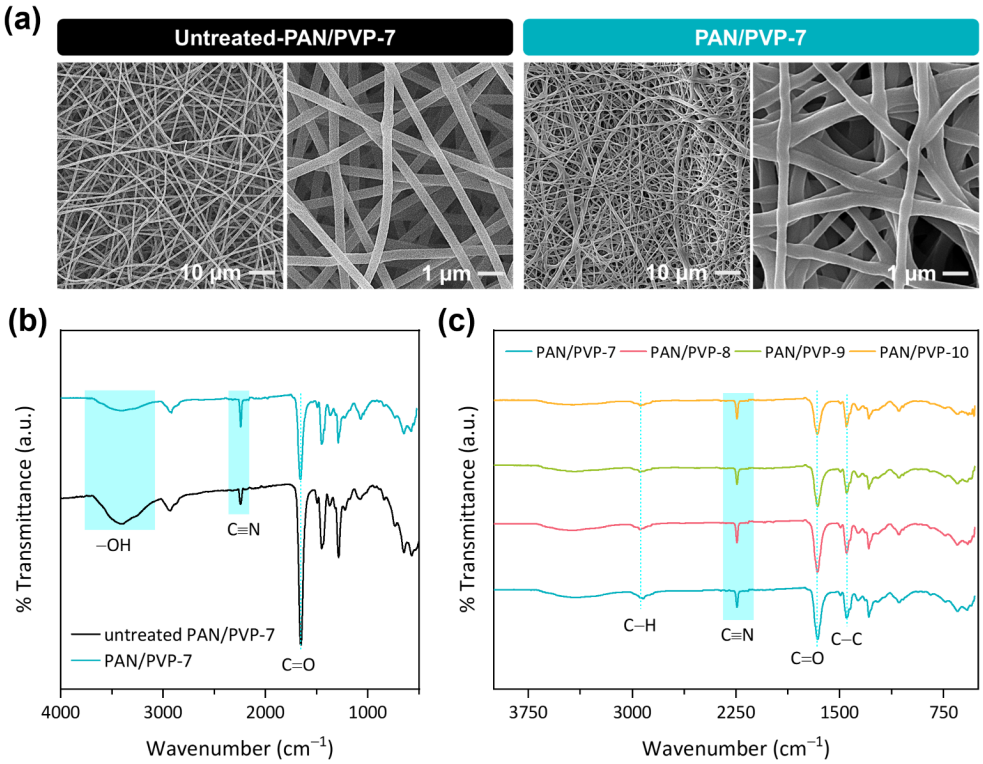

Figure 2. Morphology and FTIR spectra of electrospun PAN/PVP nanofibre membranes. (a) SEM images of untreated and post-treated PAN/PVP-7 nanofibre membrane, (b) FTIR spectra comparison between untreated and post-treated PAN/PVP-7, (c) FTIR spectra of post-treated PAN/PVP membranes with different PAN/PVP compositions.

its position and overall profile, whereas the carbonyl band of PVP in the 1660 cm^{-1} region (C=O stretching) decreases in intensity. This change in relative peak intensities suggests that the PAN component is largely preserved, while part of the PVP phase is removed or structurally degraded during the post-treatment, leading to a net reduction of PVP contributions in the infrared spectrum.

The FTIR spectra of the post-treated PAN/PVP membranes with different PAN/PVP ratios are shown in Figure 2c. All compositions display the same set of characteristic bands: the C≡N stretching of PAN at 2243 cm^{-1}, the C=O stretching of PVP at 1660 cm^{-1}, aliphatic C–H stretching at 2941 cm^{-1}, and backbone C–C/CH_2 bending vibrations around 1451 cm^{-1} [12,24,25]. As indicated by the comparison between untreated and treated PAN/PVP-7 in Figure 2b, the washing and thermal steps lead to a modest overall reduction of PVP-related signals, while preserving the PAN framework. Within Figure 2c, however, all samples have undergone the same post-treatment; therefore, the systematic decrease in the relative C=O band intensity with increasing PAN content is primarily attributed to the lower PVP concentration used during nanofibre fabrication, rather than to differential PVP removal. In other words, the spectra reflect both a slight common loss of PVP due to treatment and a compositional effect, with the dominant differences among the post-treated samples arising from their initial PVP fraction in the PAN/PVP blends [26].

The time-resolved UV–Vis spectra of MB solutions in contact with the PAN/PVP nanofibre membranes are presented in Figure 3(a–d) for the different PAN/PVP ratios. In all cases, the intensity of the main MB absorption band at around 663 nm decreases steadily with increasing contact time, reflecting a continuous reduction in MB concentration due to adsorption on the nanofibre membranes [27]. Throughout the experiment, the overall spectral profile remains essentially unchanged, with no additional bands or significant peak shifts, suggesting that MB removal occurs predominantly via adsorption rather than via photodegradation or conversion into other species [28,29]. The qualitative similarity of the spectral evolution for PAN/PVP-7, PAN/PVP-8, PAN/PVP-9, and PAN/PVP-10 indicates that all membranes are capable of effectively capturing MB from solutions, albeit with some differences in the rate and extent of peak attenuation that are examined quantitatively in the kinetic analysis. The photographs of the membranes after exposure to MB (Figure 3e) show pronounced blue coloration for all compositions, confirming dye uptake by the fibrous mats. The visual intensity and uniform distribution of the colour over the membrane surface are consistent with the progressive decrease in solution absorbance, supporting the interpretation that MB molecules are immobilized within and on the surface of the PAN/PVP nanofibre networks.

The adsorption capacities of MB as a function of contact time, calculated according to Eq. 1, are shown in Figure 4a. For all PAN/PVP compositions, MB uptake increases rapidly during the first 30–60 min and then gradually approaches an apparent plateau after approximately 180–240 min. The equilibrium adsorption capacities (q_e) are 7.448, 8.379, 6.345, and 6.805 mg g^{-1} for PAN/PVP-7, PAN/PVP-8, PAN/PVP-9, and PAN/PVP-10, respectively, with PAN/PVP-8 exhibiting the highest MB capacity and PAN/PVP-9 and PAN/PVP-10 showing slightly lower values. The kinetic behaviour of MB adsorption was analysed using the pseudo-first-order (PFO) model (Eq. 2) and the pseudo-second-order (PSO) model

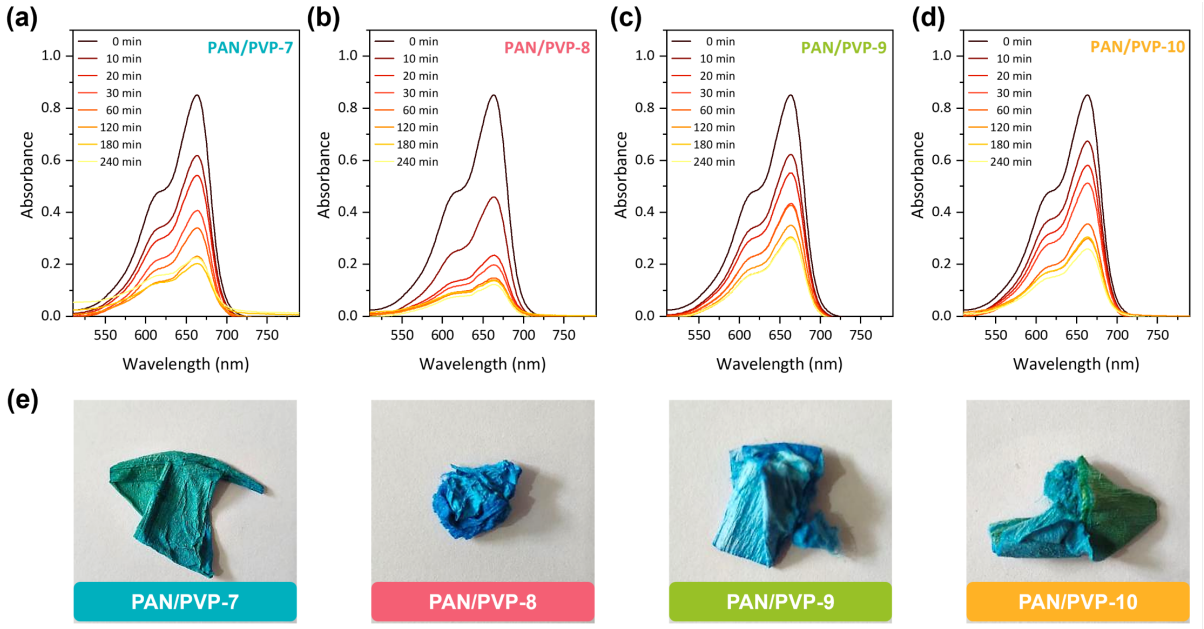

Figure 3. Adsorption of MB on PAN/PVP nanofibre membranes with different PAN/PVP ratios. (a–d) Time-resolved UV–Vis spectra of MB solutions during contact with PAN/PVP-7, PAN/PVP-8, PAN/PVP-9, and PAN/PVP-10 membranes, respectively. (e) Photographs of the corresponding PAN/PVP membranes after adsorption, evidencing different degrees of blue coloration associated with MB uptake.

(Eq. 3), as shown in Figure 4b,c. The PFO plots (Figure 4b) yield relatively low correlation coefficients ($R^2 \approx 0.26$–0.72), indicating that this model does not satisfactorily describe the experimental data. In contrast, the PSO plots (Figure 4c) exhibit excellent linearity, with R^2 values above 0.98 for all PAN/PVP compositions, demonstrating that the PSO model provides a much more appropriate representation of MB adsorption kinetics [30,31].

Figure 4d presents the adsorption capacities of CR, again calculated using Eq. 1, as a function of contact time. As for MB, the uptake increases rapidly at short times and then tends toward equilibrium; however, the equilibrium capacities are much lower: q_e = 0.778, 3.215, 2.843, and 3.316 mg g^{-1} for PAN/PVP-7, PAN/PVP-8, PAN/PVP-9, and PAN/PVP-10, respectively. The differences among compositions are modest, and all values are markedly smaller than those obtained for MB, evidencing a weaker affinity of CR for the PAN/PVP nanofibre surface under the conditions employed. The corresponding PFO and PSO kinetic analyses for CR, obtained using Eq. 2 and Eq. 3, are shown in Figure 4e,f. As in the case of MB, the PFO plots (Figure 4e) exhibit scattered data and generally lower correlation coefficients, whereas the PSO plots (Figure 4f) provide high R^2 values, typically in the range 0.93–1.00. This again indicates that the PSO model is better suited to describe the adsorption kinetics than the PFO model for all PAN/PVP compositions. The consistent preference for the PSO model for both dyes suggests that the overall adsorption rate is governed by a second-order process related to interactions between dye molecules and active sites on the nanofibre surface, rather than by a simple first-order dependence on the number of vacant sites [32].

The pronounced difference in equilibrium capacity between MB (6.345–8.379 mg g^{-1}) and CR (0.778–3.316 mg g^{-1}) can be rationalized by their molecular structures and charge characteristics [33]. Methylene blue is a cationic thiazine dye bearing positive charge in aqueous solution and aromatic rings with heteroatoms capable of interacting with polar functional groups on the PAN/PVP surface, such as C≡N from PAN and C=O from PVP [34]. These features favour electrostatic attraction and dipole–dipole interactions, leading to higher uptake [35]. Congo red, in contrast, is an anionic azo dye containing sulfonate groups and a more extended, rigid aromatic framework [36]. Under the present conditions, its negative charge and bulkier geometry are less compatible with the PAN/PVP surface, resulting in weaker overall interactions and lower adsorption capacities [37].

Taken together with the relatively small morphological differences among the fibres and the similar FTIR signatures, the equilibrium and kinetic results derived from Eq. 1–3 indicate that all PAN/PVP compositions follow a broadly similar adsorption mechanism dominated by surface interactions. Within this common mechanism, the chemical nature and charge distribution of the dye molecules, rather than subtle variations in nanofibre morphology induced by PAN/PVP ratio and post-treatment, play the dominant role in determining the absolute adsorption capacity.

4. CONCLUSIONS

PAN/PVP nanofibre membranes with varying polymer ratios were successfully fabricated by electrospinning and subsequently subjected to hot-water soaking at 80 °C followed by thermal treatment at 200 °C. SEM and FTIR analyses confirmed the coexistence of both polymer components after post-treatment and revealed only modest morphological and chemical variations among the different compositions. FTIR, in particular, showed a decrease in the PVP-related C=O band while the PAN C≡N signal remained essentially unchanged, indicating partial removal of PVP-rich, water-soluble domains during soaking and heating, but not complete depletion of PVP from the fibrous matrix. Batch adsorption experiments

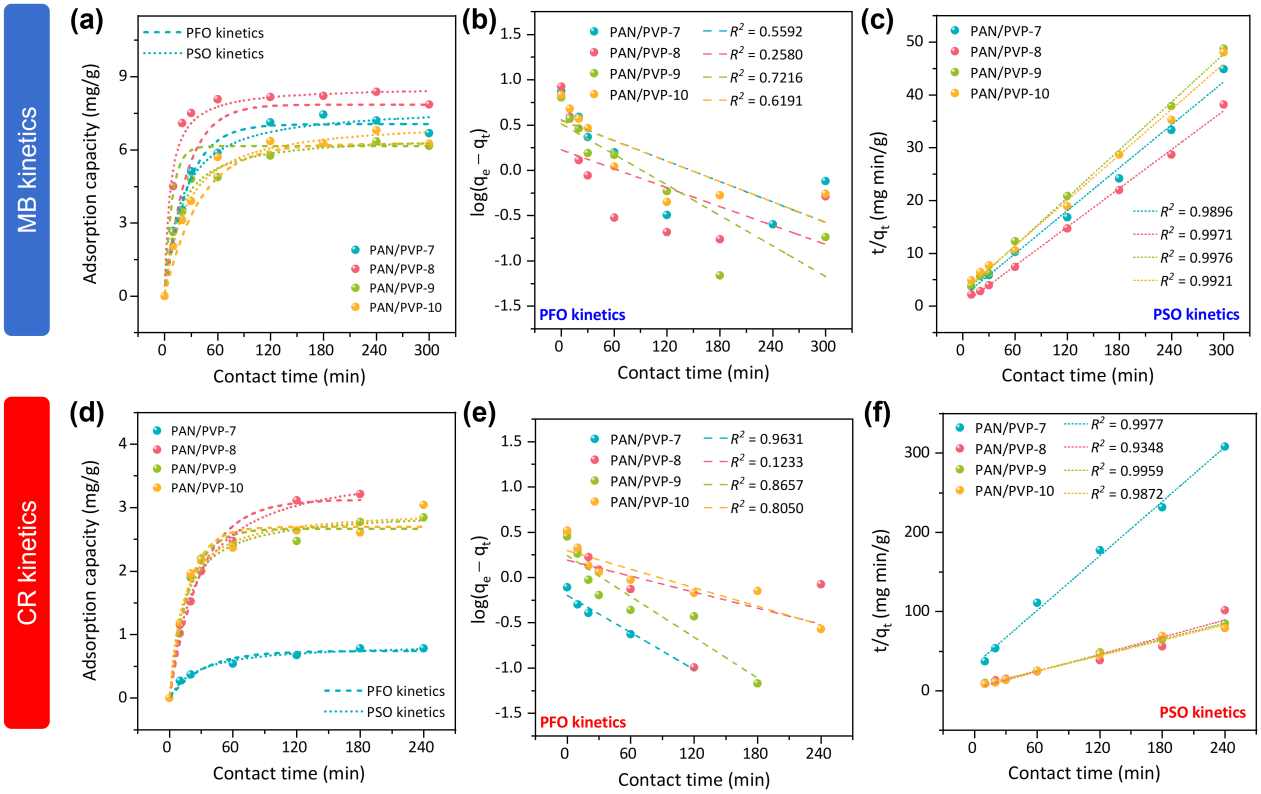

Figure 4. Kinetic analysis of MB and CR adsorption on PAN/PVP nanofibre membranes with different PAN/PVP ratios. (a) Experimental MB adsorption capacity as a function of contact time together with PFO and PSO model fits. (b,c) Linear PFO and PSO plots for MB adsorption, respectively. (d) Experimental CR adsorption capacity as a function of contact time with PFO and PSO model fits. (e,f) Linear PFO and PSO plots for CR adsorption, respectively.

demonstrated that all membranes preferentially adsorb MB over CR, with the highest equilibrium capacity of 8.38 mg g^{-1} for MB obtained on the PAN/PVP-8 membrane and the highest CR capacity of 3.32 mg g^{-1} obtained on the PAN/PVP-10 membrane, thereby highlighting the dominant role of dye charge and molecular structure in governing adsorption behaviour. Although one composition exhibits slightly higher capacities for each dye, the overall differences in adsorption performance among the four PAN/PVP ratios remain moderate, reflecting broadly similar behaviour across the series. Kinetic analysis based on the PFO and PSO models showed that the pseudo-second-order model provides an excellent fit for both MB and CR uptake, supporting a rate-limiting step governed by surface–dye interactions at active sites on the nanofibre surface. Taken together, these results suggest that, within the composition and post-treatment window explored here, partial PVP removal and variation in PAN/PVP ratio produce only incremental improvements, and that more substantial enhancement of adsorption performance will likely require targeted surface modification or functionalization rather than simple adjustment of blend composition. Future work should therefore focus on introducing specific functional groups or tailored active sites to further enhance dye affinity and selectivity.

FUNDING ACKNOWLEDGEMENT

This study receives no funding.

DATA AVAILABILITY STATEMENT

The datasets generated during and/or analysed during the current study are available from the corresponding author on reasonable request.

AUTHOR CONTRIBUTIONS

IRH: Conceptualization, Writing – Original Draft Preparation, Writing – Review & Editing, Supervision. ATLT: Investigation, Writing – Original Draft Preparation. HRPS: Investigation. AF: Formal analysis, Writing – Review & Editing. AP: Formal analysis, Writing – Review & Editing. All authors approved the final manuscript.

CONFLICT OF INTEREST

The authors declare that there are no conflicts of interest.

REFERENCES

[1] S. Sudarshan, S. Harikrishnan, G. RathiBhuvaneswari, V. Alamelu, S. Aanand, A. Rajasekar, M. Govarthanan, Impact of textile dyes on human health and bioremediation of textile industry effluent using microorganisms: current status and future prospects, *Journal of Applied Microbiology* 134 (2023) lxac064. doi:10.1093/jambio/lxac064.

[2] A. Silina, A. El Achari, F. Salaün, Metal-organic framework electrospun nanofibers in application to dye removal from textile wastewaters: A review, *Journal of Environmental Chemical Engineering* 12 (2024) 114819. doi:10.1016/j.jece.2024.114819.

[3] D. Dhruv Patel, S. Bhatt, Environmental pollution, toxicity profile, and physico-chemical and biotechnological

approaches for treatment of textile wastewater, *Biotechnology and Genetic Engineering Reviews* 38 (2022) 33–86. doi:10.1080/02648725.2022.2048434.

[4] N.Y. Donkadokula, A.K. Kola, I. Naz, D. Saroj, A review on advanced physico-chemical and biological textile dye wastewater treatment techniques, *Reviews in Environmental Science and Bio/Technology* 19 (2020) 543–560. doi:10.1007/s11157-020-09543-z.

[5] Y.S. Hao, N. Othman, M.A.A. Zaini, Methylene blue and Congo red removal by activated carbons: A current literature, Acta Universitatis Sapientiae, *Agriculture and Environment* 14 (2022) 29–44. doi:10.2478/ausae-2022-0003.

[6] S.S. Vedula, G.D. Yadav, Wastewater treatment containing methylene blue dye as pollutant using adsorption by chitosan lignin membrane: Development of membrane, characterization and kinetics of adsorption, *Journal of the Indian Chemical Society* 99 (2022) 100263. doi:10.1016/j.jics.2021.100263.

[7] N.S.L. Dissanayake, M.A. Pathirana, N.D. Wanasekara, B. Mahltig, G.K. Nandasiri, Removal of Methylene Blue and Congo Red Using a Chitosan–Graphene Oxide-Electrosprayed Functionalized Polymeric Nanofiber Membrane, *Nanomaterials* 13 (2023) 1350. doi:10.3390/nano13081350.

[8] S. Dutta, B. Gupta, S.K. Srivastava, A.K. Gupta, Recent advances on the removal of dyes from wastewater using various adsorbents: a critical review, *Materials Advances* 2 (2021) 4497–4531. doi:10.1039/d1ma00354b.

[9] H.N. Hamad, S. Idrus, Recent Developments in the Application of Bio-Waste-Derived Adsorbents for the Removal of Methylene Blue from Wastewater: A Review, *Polymers* 14 (2022) 783. doi:10.3390/polym14040783.

[10] O.P. Murphy, M. Vashishtha, P. Palanisamy, K.V. Kumar, A Review on the Adsorption Isotherms and Design Calculations for the Optimization of Adsorbent Mass and Contact Time, *ACS Omega* 8 (2023) 17407–17430. doi:10.1021/acsomega.2c08155.

[11] M.A. Pathirana, N.S.L. Dissanayake, N.D. Wanasekara, B. Mahltig, G.K. Nandasiri, Chitosan-Graphene Oxide Dip-Coated Polyacrylonitrile-Ethylenediamine Electrospun Nanofiber Membrane for Removal of the Dye Stuffs Methylene Blue and Congo Red, *Nanomaterials* 13 (2023) 498. doi:10.3390/nano13030498.

[12] H. Fakhry, M. El-Sonbati, B. Omar, R. El-Henawy, Y. Zhang, M. EL-Kady, Novel fabricated low-cost hybrid polyacrylonitrile/polyvinylpyrrolidone coated polyurethane foam (PAN/PVP@PUF) membrane for the decolorization of cationic and anionic dyes, *Journal of Environmental Management* 315 (2022) 115128. doi:10.1016/j.jenvman.2022.115128.

[13] S. T. M., A.B. Arshad, P.T. Lin, J. Widakdo, M. H. K., H.F.M. Austria, C.C. Hu, J.Y. Lai, W.S. Hung, A review of recent progress in polymeric electrospun nanofiber membranes in addressing safe water global issues, *RSC Advances* 11 (2021) 9638–9663. doi:10.1039/d1ra00060h.

[14] A. Rianjanu, K.D.P. Marpaung, E.K.A. Melati, R. Aflaha, Y.G. Wibowo, I.P. Mahendra, N. Yulianto, J. Widakdo, K. Triyana, H.S. Wasisto, T. Taher, Integrated adsorption and photocatalytic removal of methylene blue dye from aqueous solution by hierarchical Nb2O5@PAN/PVDF/ANO composite nanofibers, *Nano Materials Science* 6 (2024) 96–105. doi:10.1016/j.nanoms.2023.10.006.

[15] R. Aflaha, H. Afiyanti, Z.N. Azizah, H. Khoirudin, A. Rianjanu, A. Kusumaatmaja, R. Roto, K. Triyana, Improving ammonia sensing performance of quartz crystal microbalance (QCM) coated with nanofibers and polyaniline (PANi) overlay, *Biosensors and Bioelectronics: X* 13 (2023) 100300. doi:10.1016/j.biosx.2022.100300.

[16] R. Aflaha, L.A. Putri, C.N. Maharani, A. Rianjanu, R. Roto, H.S. Wasisto, K. Triyana, Tuning a Superhydrophobic Surface on an Electrospun Polyacrylonitrile Nanofiber Membrane by Polysulfone Blending, *ACS Omega* 9 (2024) 29840–29847. doi:10.1021/acsomega.4c03554.

[17] R. Aflaha, C.N. Maharani, L.A. Putri, Y.D. Prabowo, I. Rahman, T. Taher, A. Rianjanu, R. Roto, H.S. Wasisto, K. Triyana, A superhydrophobic and heat-resistant PAN/PSU/PTFE composite nanofiber membrane for high-efficiency PM _1.0 and PM _2.5 filtration, *Materials Advances* 5 (2024) 9731–9743. doi:10.1039/D4MA00841C.

[18] R. Aflaha, L.A. Putri, A. Farrel, S. Anzinger, A. Rianjanu, N. Yulianto, M. Fueldner, R. Roto, E. Peiner, H.S. Wasisto, K. Triyana, Crafting high-temperature stable and hydrophobic nanofiber membranes for particulate matter filtration, *Communications Materials* 6 (2025) 87. doi:10.1038/s43246-025-00799-y.

[19] L. Katriani, R. Aflaha, C.N. Maharani, F. Naafi'ah Salsabila, A.H. As'ari, A. Rianjanu, P. Nurwantoro, R. Roto, K. Triyana, Quartz Crystal Microbalance Coated with a Polyvinylpyrrolidone Microfiber Active Layer as a High-Performance Acetic Acid Gas Sensor, *Langmuir* 41 (2025) 4632–4640. doi:10.1021/acs.langmuir.4c04474.

[20] R. Aflaha, E.N.S. Putri, C.N. Maharani, L. Katriani, A.H. As'ari, A. Rianjanu, W.B.K. Putri, K. Triyana, R. Gupta, R. Roto, QCM-based ammonia gas sensors with electrospun polymer-based nanofibers for liver and kidney disease detection: a mini-review, *Journal of Materials Chemistry B* 13 (2025) 13589–13607. doi:10.1039/D5TB00842E.

[21] G. Zhou, L. Jiang, G. Chen, Y. Ma, Y. Wang, R. Liu, Electrospun porous polyacrylonitrile/polyvinylpyrrolidone nanofiber membrane with ultra-hydrophilic and high moisture-permeability for dust personal protection, *Journal of Environmental Chemical Engineering* 12 (2024) 113524. doi:10.1016/j.jece.2024.113524.

[22] Y. Kang, J. Chen, S. Feng, H. Zhou, F. Zhou, Z.X. Low, Z. Zhong, W. Xing, Efficient removal of high-temperature particulate matters via a heat resistant and flame retardant thermally-oxidized PAN/PVP/SnO2 nanofiber membrane, *Journal of Membrane Science* 662 (2022) 120985. doi:10.1016/j.memsci.2022.120985.

[23] H. Wu, Y. Wang, X. Zhang, W. Xing, L. Li, H. Wang, L. Huang, J. Tang, PAN/ CB spheres modified PAN/PVP dual amphiphilic porous nanofiber membranes for high-performance oil-water separation, *Colloids and Surfaces A: Physicochemical and Engineering Aspects* 726 (2025) 137768. doi:10.1016/j.colsurfa.2025.137768.

[24] O.A.A.Q. Mahmood, B.I. Waisi, Crystal violet dye removal from aqueous water using polyacrylonitrile precursor beads, *Materials Today: Proceedings* 42 (2021) 2185–2192. doi:10.1016/j.matpr.2020.12.303.

[25] J. Chokki, G. Darracq, P. Poelt, J. Baron, H. Gallard, M. Joyeux, B. Teychené, Investigation of Poly(ethersulfone)/Polyvinylpyrrolidone ultrafiltration membrane degradation by contact with sodium hypochlorite through FTIR mapping and two-dimensional correlation spectroscopy, *Polymer Degradation and Stability* 161 (2019) 131–138. doi:10.1016/j.polymdegradstab.2019.01.017.

[26] F. Wang, Z. Zhang, Y. Yan, Z. Shen, Q. Wang, R. Gerhard, Surface Reconstruction on Electro-Spun PVA/PVP Nanofibers by Water Evaporation, *Nanomaterials* 12 (2022) 797. doi:10.3390/nano12050797.

[27] N. Mohammad, Y. Atassi, Adsorption of methylene blue onto electrospun nanofibrous membranes of polylactic acid and polyacrylonitrile coated with chloride doped polyaniline, *Scientific Reports* 10 (2020) 13412. doi:10.1038/s41598-020-69825-y.

[28] M. Ulfa, S.L. Oktaviani, B. Mulyani, N.A. Sholeha, Metal Oxide for Fast Adsorption System in the Methylene Blue Removal, *Indonesian Journal of Chemistry* 25 (2025) 619. doi:10.22146/ijc.92617.

[29] N.A. Bakar, N. Othman, Z.M. Yunus, W.A.H. Altowayti, M. Tahir, N. Fitriani, S.N.A. Mohd-Salleh, An insight review of lignocellulosic materials as activated carbon precursor for textile wastewater treatment, *Environmental Technology & Innovation* 22 (2021) 101445. doi:10.1016/j.eti.2021.101445.

[30] J. Wang, X. Guo, Adsorption kinetics and isotherm models of heavy metals by various adsorbents: An overview, *Critical Reviews in Environmental Science and Technology* 53 (2023) 1837–1865. doi:10.1080/10643389.2023.2221157.

[31] L. Largitte, R. Pasquier, A review of the kinetics adsorption models and their application to the adsorption of lead by an activated carbon, *Chemical Engineering Research and Design* 109

(2016) 495–504. doi:10.1016/j.cherd.2016.02.006.

[32] D.A. Ali, F.M. Abdalla, D.A. Gamil, H.A. Elsawy, Isotherm and kinetics studies for the adsorption of methylene blue and methyl red dyes from aqueous solutions using chitosan, *ARPN J. Eng. Appl. Sci* 16 (2021) 732–741.

[33] L. Zhang, L. Yang, J. Chen, W. Yin, Y. Zhang, X. Zhou, F. Gao, J. Zhao, Adsorption of Congo Red and Methylene Blue onto Nanopore-Structured Ashitaba Waste and Walnut Shell-Based Activated Carbons: Statistical Thermodynamic Investigations, Pore Size and Site Energy Distribution Studies, *Nanomaterials* 12 (2022) 3831. doi:10.3390/nano12213831.

[34] M. Soleimani Fard, N. Samadani Langeroodi, M. Javan, A. Dehno Khalaji, The Removal of Methylene Blue from Aqueous Solutions Using CuFe_2O_4/PVP Nanocomposite: An Experimental and Theoretical Study, *Iranian Journal of Soil and Water Research* 55 (2025) 2109–2124. doi:10.22059/ijswr.2024.379082.669764.

[35] Fatiatun, S.A. Bakar, A. Mohamed, H.H. Kusuma, Muqoyyanah, R. Mohamat, V.V. Kumar, K. Ali, R. Nuryadi, M.N.A. Azis, M.K. Ahmad, M.H. Mamat, M.H.D. Othman, High Methylene Blue Adsorption Efficiency of Cellulose Acetate-Based Electrospun Nanofiber Membranes Modified with Graphene Oxide and Zeolite, *International Journal of Environmental Research* 19 (2025) 18. doi:10.1007/s41742-024-00683-6.

[36] A. Strebel, M. Behringer, H. Hilbig, A. Machner, B. Helmreich, Anionic azo dyes and their removal from textile wastewater through adsorption by various adsorbents: a critical review, *Frontiers in Environmental Engineering* 3 (2024) 1347981. doi:10.3389/fenve.2024.1347981.

[37] A. Khan, M. Arif, Z. Han, Y. Xie, C. Ni, Mechanism and performances of methyl orange and Congo red adsorption by MnO2–PVP composite, *Water Practice & Technology* 19 (2024) 1047–1060. doi:10.2166/wpt.2024.032.

